Mine Water and the Environment
https://doi.org/10.1007/s10230-021-00827-6

TECHNICAL ARTICLE

Analysis of Acid Drainage Flow Zones in a Rocky Massif in a Uranium Mine from Structural and Geophysical Diagnoses

Pedro Lemos Camarero[1] · César Augusto Moreira[1] · Débora Andrade Targa[1] · Beatriz Guzzo Duz[1] · Henrique Garcia Pereira[2]

Received: 13 April 2021 / Accepted: 11 September 2021

Abstract
During its 13 years of non-continuous operation, the Osamu Utsumi Mine has generated serious environmental impacts. This mining complex is now attempting to decommission this uranium mine to reduce its environmental liabilities. As part of a hydrogeological analysis of the old Osamu Utsumi Mine pit area, a geophysical investigation was carried out along each front of the mine pit using electrical resistivity tomography and a dipole–dipole array. The lithology described in each front, the physical access, and data from monitoring wells also contributed to the geophysical interpretation and, hence, the hydrogeological analysis. The field results and geochemical data from monitoring wells enabled us to distinguish areas where water was flowing through fractures in the massif and areas with more acidic water, with electrical resistivity values less than 15 Ω m.

Keywords Electrical resistivity tomography · Sulfides · Mine decommissioning · DC resistivity · Hydrogeology · Fractured aquifer

Introduction

In the mid-1940s, there was a growing worldwide demand for radioactive minerals for nuclear energy production. In this historical context, the first research projects were initiated in Brazilian territory in the beginning of the 1950s. One of the targets of mineral research was the alkaline mass of Poços de Caldas in southeastern Brazil. Several occurrences of uranium and thorium were recorded; the Cercado deposit was the most promising of the targets and the site of the first uranium mine in Brazil, called Osamu Utsumi (Pires 2013). The Osamu Utsumi mine was Brazil's main uranium mine for many years. However, as newly discovered deposits showed better grades of uranium, the mining complex started to present a high cost-benefit ratio. INB (Indústiras Nucleares do Brasil)—a state-owned company that monopolizes the exploitation of radioactive minerals in Brazil, decided in 1995 to end activities in this mining complex in Poços de Caldas and to invest in deposits with higher grades in other locations in the country (Moreira et al. 2020). The mine is currently being decommissioned (Targa et al. 2019).

Exposure of sulfide zones to atmospheric contact and rainwater led to one of the most common environmental problems in similar areas, a phenomenon known as acid mine drainage (AMD). Deposits of radioactive minerals are an additional aggravating factor with respect to AMD, as metals such as uranium can be mobilized in highly acidic environments.

At the Osamu Utsumi mine, acidic waters are pumped to a conventional treatment plant, where they are treated with calcium oxide (CaO) or calcium hydroxide ($Ca(OH)_2$) to increase the pH, which induces the precipitation of most

✉ Pedro Lemos Camarero
camarero@folha.com.br

César Augusto Moreira
moreirac@rc.unesp.br

Débora Andrade Targa
debora.targa@gmail.com

Beatriz Guzzo Duz
beatrizduz@gmail.com

Henrique Garcia Pereira
ique_garcia@hotmail.com

[1] Geosciences and Exact Sciences Institute (IGCE), São Paulo State University (UNESP, 24-A Ave, 1515, Bela Vista, Rio Claro, São Paulo State 13506-900, Brazil

[2] Federal University of Paraná (UFPR), XV de Novembro Str, 1299, Downtown, Curitiba, Paraná State 80060-000, Brazil

Published online: 05 October 2021

metallic and radioactive elements, but results in a waste, calcium diuranate, locally called DUCA (Franklin 2007). The metals with the highest concentrations in the study area are Mn, Fe, Al, and Zn. Effluents from the wastewater treatment plant used to be discharged into a tailings impoundment, but they are currently disposed inside the open pit, which is an unsustainable long-term process.

Geophysics can contribute to mining and hydrogeological studies (Côrtes et al. 2016; Frid et al. 2017; Gélis et al. 2010; Gélis et al. 2015; Ghosal et al. 2020; Handam et al. 2014; Khalil et al. 2018; Obiadi et al. 2013; Oliveti and Cardarelli 2019; Moreira et al. 2016, 2018; Zhang et al. 2018). Using methods such as direct-current (DC) resistivity, it is possible to identify the main structures in a fractured aquifer where there is a contrast of physical properties due to the percolation of water. Rocky massifs have secondary permeability associated with fracturing, through which water percolates. Mineralized water tends to be a good conductor of electricity, which promotes a geophysical signature of low resistivity. Geophysical methods combined with geological mapping helps to identify and dimension the main areas contributing AMD (Buselli and Lu 2001; Ebraheem et al. 1990; Epov et al. 2017; Gómez-Ortiz et al. 2010; Korneeva et al. 2016; Lghoul et al. 2012; Martín-Crespo et al. 2018; Martinez-Pagan et al. 2009, 2013, 2021; Merkel 1972; Placencia-Gómez et al. 2010; Poisson et al. 2009; Rucker et al. 2009; Targa et al. 2019; Yuval and Oldenberg 1996). Others geophysical surveys of uranium deposits are reported in Legault et al. 2008; Mandal et al. 2013; Mwenifumbo et al. 2004; Tuncer et al. 2006.

This study identified zones responsible for the process of generating acid mine drainage inside a rock massif at an open pit uranium mine, with the objective of proposing actions to reduce environmental impacts and technical solutions for long term environmental sustainability. The set of diagnostic methods for AMD generation and flow areas provided satisfactory results despite a complex flow system.

Study Area and Geologic Context

The Osamu Utsumi mine is located in the Poços de Caldas alkaline complex, located in the south of the state of Minas Gerais, in southeastern Brazil (Fig. 1). The geological complex is composed of a circular volcanic structure (a caldera), with an area of ≈800 km^2 and a diameter of 35 km. It sits ≈500 m above the surrounding regions.

The regional geological context is represented by phonolites, nepheline syenites, supracrustal pyroclastic rocks, and clastic sedimentary rocks (Garda 1990). The structural tectonic evolution of the Poços de Caldas massif is compatible with the volcanic caldera formation model (Holmes et al. 1992). The magmatic plume generated different tectonic stages that involved stages of basement uplift and the

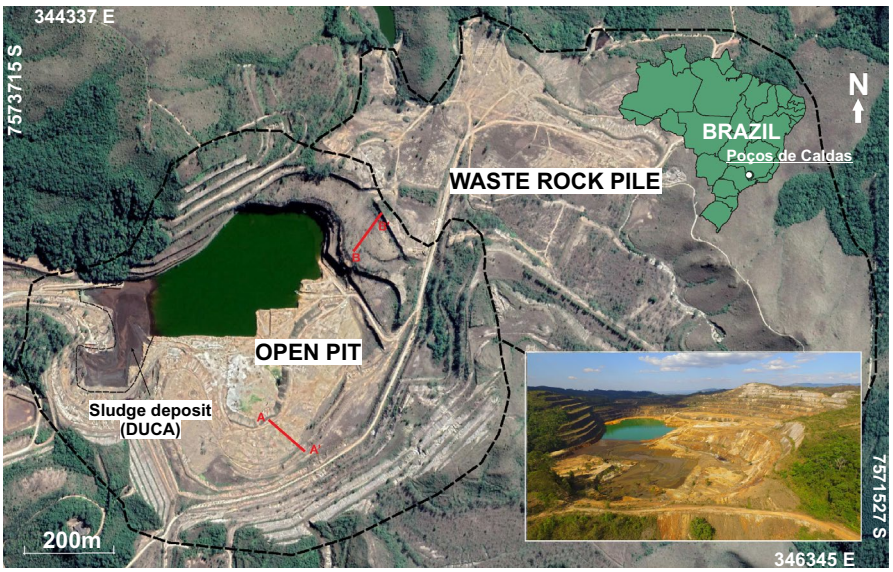

Fig. 1 The study area

appearance of several distensive fractures, intense magmatic activity, followed by collapse and abatement of the the central portion of the dome, with intense tectonism and hydrothermal events associated with volcanic breaches. This last stage in the evolution of the caldera was essential for the mineralisation of the Osamu Utsumi mine.

The entire rise and subsidence of the surrounding rocks and the massif itself generated an intense regional fracturing. This fracturing pattern follows two main directions, N40E and N60W (Fraenkel et al. 1985). To a lesser extent, there may be fractures in the N–S direction. The fracturing pattern is altered close to the edges of the caldera, due to its curvature.

The mineralized bodies at the Osamu Utsumi mine are installed in a conical tectonic breaccia chimney, with surface dimensions of 1200 m × 600 m (Biondi 2015). The genesis of the deposit occurred in two main stages: hydrothermalism, responsible for the primary mineralization, and weathering processes, responsible for the secondary mineralization.

The primary mineralization occurred in magmatic pulses of nepheline syenites at high pressures, which forced the migration of the fluid part of the magma in the rocks. At this stage, uranium was deposited in a widespread manner in the pores of the rocks as pitchblende/uraninite. Fluorite and pyrite were also been deposited in veins (Waber et al. 1992).

Weathering and secondary mineralization was induced by the intense fracturing and high permeability of the rocks in the breach, which permitted the oxidation of pyrite and the dissolution of salts and, consequently, the generation of acidic waters. The acidic water leached part of the disseminated uranium and concentrated part of it in nodules in the oxidation/reduction zone and in fractures. The ore is also concentrated in the fractured areas and in the clays that fill the fractures (Fig. 2).

The mining method adopted during the operation period was an open pit mine. The pit has the shape of an ellipse with diameters of 1200 m (NE–SW) and 800 m (NW–SE). The exploitation method was bench system, in which the heights of the benches varied from 16 m in zones of sterile material to 2 m in mineralized zones (Franklin 2007). The movement of material generated during the mine operation resulted several environmental damages, most important, the acid mine drainage (AMD).

The mining operation was carried out by breaking rocks using the technique of drilling and blasting by explosives. The energy from these blasts may have increased the persistence of fracture system in the massif, in addition to the generation of secondary fracturing. The option of the open pit mining method generated a large movement of material from the pit - according to the estimative by Cipriani (2002), 94.5×10^6 tons of soil and rock were moved, an additional factor to relieve tension in the massif.

The acidic waters come from the percolation of rainwater through the waste rock piles and through the pit massif itself. Part of this water arises naturally at the water table in the open pit region. The interaction with mineralized zones that still exist at the site promotes the genesis of acid drainage (Fernandes et al. 1995). And one of the determining factors for this problem is that part of the ore, which is also associated with occurrences of sulfides, occurs in fractures of the massif where the permeability of the rock occurs (Fig. 3a and b).

Currently acidic waters are treated by traditional methods of neutralizing acidic pH with the addition of lime (CaO) or calcium hydroxide ($Ca(OH)_2$) in order to promote an increase in pH. The result of the chemical reaction generates a particulate residue with precipitates calcium diuranate and metal hydroxides, various in a calcium sulfate matrix and manganese rich preciptate in addition to metallic and

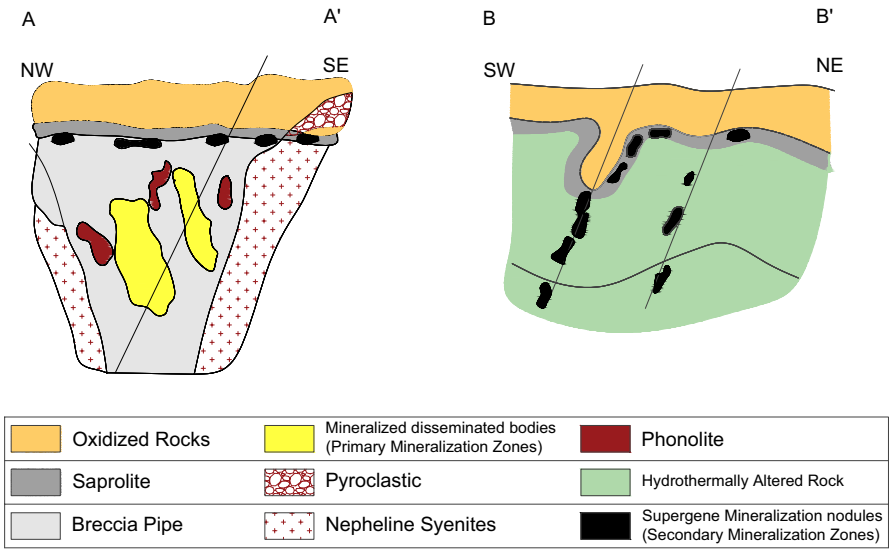

Fig. 2 Schematic profile with the two main processes of genesis of the Osamu Utsumi mine (Adapted from Magno Jr. 1985)

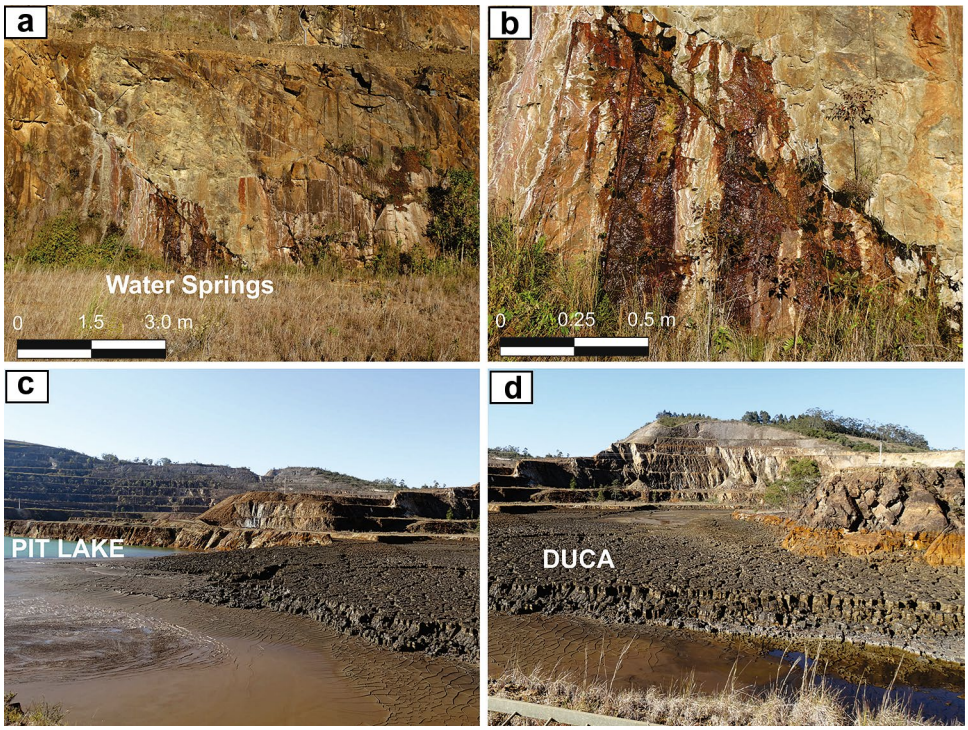

Fig. 3 a and b Detail of fractures with water flow; c and d Image of the sludge deposit (DUCA) in the pit lake

radioactive metals. This sludge residue is called calcium diuranate (DUCA) and has been deposited in the mine pit (Fig. 3c and d). This solution is not sustainable in the long term, as each year the amount of waste in the pit increases, which makes the treatment of acidic waters in the mining complex a palliative measure.

Materials and Methods

For structural analysis of the mine pit, a survey of structural measurements of the attitudes of the main fracture planes of the pit rocks was carried out using a Brunton geological compass and a Clar notation system (dip direction/dip). The local magnetic declination is 21° 37′. The measurements were collected during the dry period (Chart 1); however, it was still possible to verify water flow in several fractures and flow indications in several others areas in the massif.

Due to the pit dimensions, the work fronts were divided into four main fronts based on the cardinal points (NE, SE, SW, and NW). In all, 811 structural measures were carried out. Data processing was performed using the OpenStereo software and the data was presented as half circles with the trends of strike and dip direction. This local structural pattern was compared with the regional structural pattern (Fig. 4).

Structural geology data serves as a basis for understanding geophysical data in addition to contributing to the

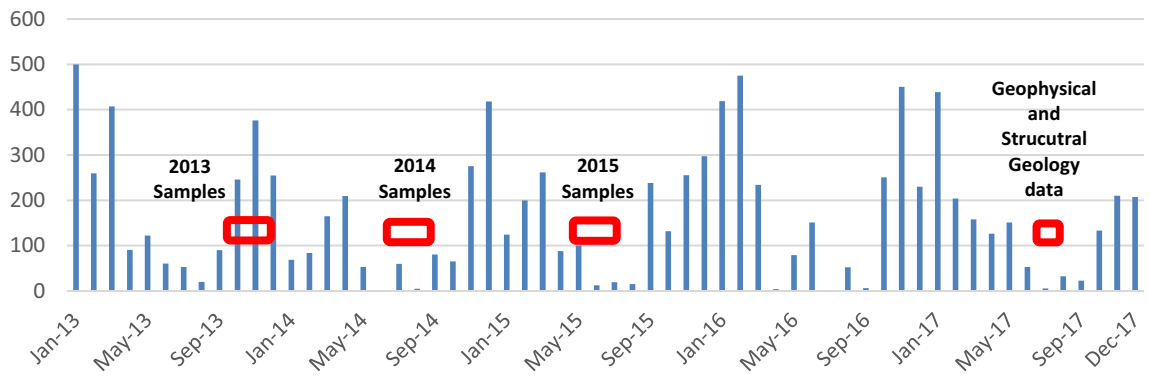

Fig. 4 Rainfall regime (in mm) and data collection campaigns

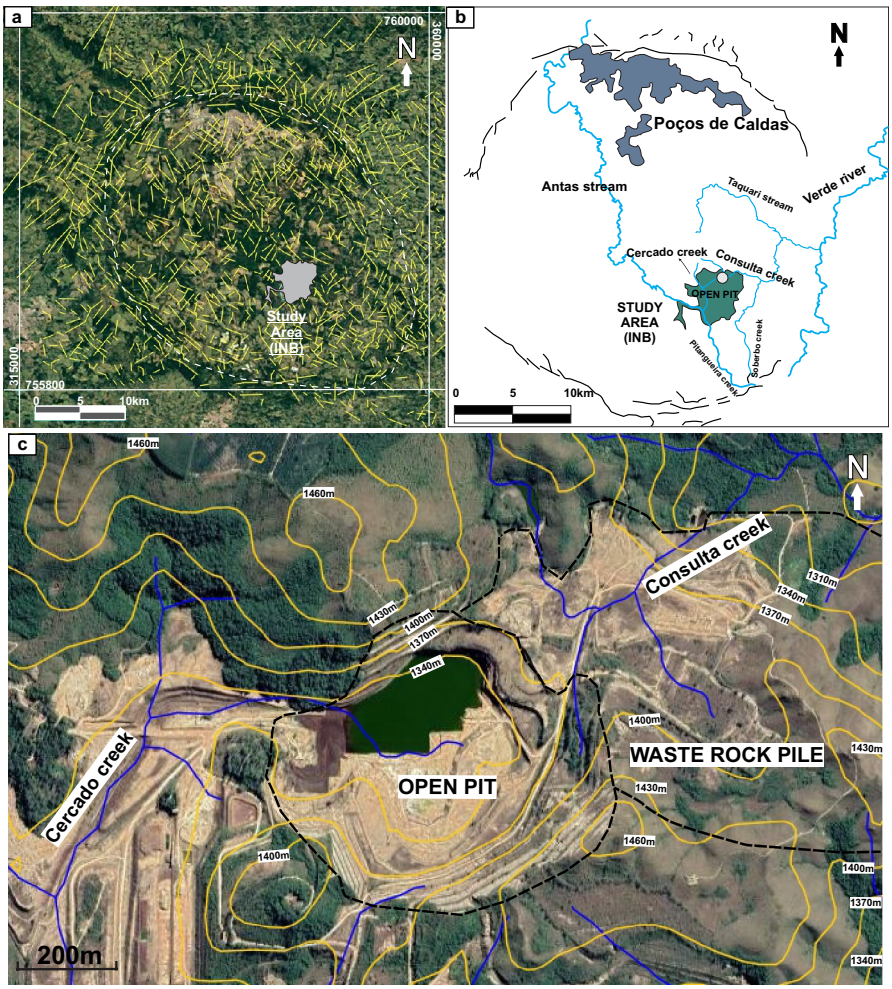

Fig. 5 **a** The main structural lineaments of the Poços de Caldas massif (in yellow); the edge of the Poços de Caldas alkaline massif (in white), adapted from Moreira et al. 2007. **b** Surface hydrology. **c** Local relief and the two main drainages around the pit: Cercado and Consulta Creeks

understanding of the underground water flow regime in the mine pit. Figure 4a presents an analysis of the combined Landsat-TM and RADAR images described in Moreira et al. (2007) for understanding and identifying the regional outlines and faults of the Caldas alkaline massif. The yellow lines represent straight drainage patterns in the massif that are associated with the alkaline intrusión, which generated a ring dyke at the edges of the massif. At these points, there are lines that follow the direction of the intrusion, representing typical features of magmatic intrusions and igneous bodies. However, most of the lineaments are in the NE–SW and NW directions, which is consistent with what is known of the area (Moreira et al. 2007; Targa et al. 2019).

Local tectonics affected the drainage pattern of the massif. There are two main drainages from the massif: the Antas Stream and the Verde River (Fig. 4b). The open pit mine is on a watershed that divides the basins of Cercado Creek to the east and Consulta Creek to the west (Fig. 4c). The waters of the Cercado creek converge to the east towards the Antas, while the waters of the Consulta converge to the west, flowing towards the Verde. DC resistivity was used for the detection of the three-dimensional bodies and electrical properties of the soil, in addition to the study of the massif's discontinuities. This method is routinely used in mineral research, geotechnics, hydrogeology and in environmental studies (Kearey et al. 2002).

In the DC resistivity method, continuous or very low frequency electric currents are introduced into the soil through a pair of electrodes and the resulting potential differences are measured on the surface by means of another pair of electrodes, in the area of influence of the electric field. The depth of investigation is governed by the spacing between the electrodes. Deviations from the pattern of potential differences expected from homogeneous soil provide information on the shape and electrical properties of surface heterogeneities (Kearey et al. 2002). From the intensity of the current that runs through the basement (I, in amperes), the geometry of the arrangement of electrodes (K), and the potential difference measured by electrodes receivers (ΔV), it is possible to calculate the apparent resistivity (ρa) value due to heterogeneity using the equation:

$$\rho a = K\frac{\Delta V}{I(A)}\text{Ohm}\,.\,\text{m}$$

Resistivities are commonly controlled by rock porosity and by the salinity of the pore waters. However, clay minerals are electrically polarized and rocks containing them are highly conductive when even slightly moist (Moon et al. 2006).

The geophysical data were processed on RES2DINV software, presented as distance × depth sections, as an electrical resistivity inversion model (Loke and Baker 1996). This program is designed for processing large data sets in two dimensions acquired by means of electrical imaging. The inversion process consists of a series of rectangular blocks; the layout of the blocks is linked to the distribution of data points on a pseudo-section, i.e. the section generated by the in-depth theoretical field data. The distribution and size of the blocks are generated automatically by the program according to the distribution of data points. The depth of the bottom row of blocks is set to be approximately equal to the equivalent depth of investigation of points with the largest gap between electrodes (Edwards 1977). The direct modeling technique is used to calculate the values of apparent resistivity, while the technique of nonlinear optimization for least squares is used in an inversion routine (Degroot-Hedlin and Constable 1990; Loke and Baker 1996).

Four electrical resistivity tomography (ERT) surveys were performed in the mine pit, one in each quadrant. The ERTs on the NW, NE, and SE fronts were 400 m long, while the ERT SW was 300 m long; the spacing between electrodes adopted for all ERT surveys was 10 m. The equipment used was an ABEM Terrameter LS resistivity meter with 84 electrodes and 250 W of power, which was calibrated for resistivity measurements through periodic cycles of electric current at low frequency, a procedure that allows filtering of any acquired signal noise (ABEM 2012). The electrical tomography lines were performed by means of a dipole-dipole arrangement. In general, the red and yellow areas represent higher resistivity values, while the cold colors, such as blue, had lower resistivities.

It is important to note that the data acquisition occurred during the drought period, with the aim of detaching any flow coming directly from rains, so that the flow zones coming from the fractured aquifer could be recognized. At several points in the pit, it was possible to recognize the presence of water from fracture systems of the rock massif. In addition there are signs of water flow in the dry fractures, such as the presence of kaolinite (due to chemical weathering) and vegetation. On the NW and SE fronts, constant water flows were observed at the intersectons of fracture planes.

The rocks, when unsaturated, generally have a relatively high resistivity value (> 400 Ω m), but factors such as the degree of alteration, fracturing, the presence of specific minerals, and water percolation tend to decrease electrical resistivity (McNeill 1980). Lithological differentiation is important for the interpretation of the data; different responses were expected relative to the electrical conductivity of each lithology. Figure 5 integrates lithologic elements and the spatial positioning of the geophysical acquisition lines over the study area. The contrast will be clearer in the geophysical lines in which there is marked lithological contact. Breccia are rocks that have undergone a high degree of stress and in general tend to have a high degree of fracturing and alteration, factors that result in low resistivity values.

In the case of AMD there are several ions dissolved in the water, specially SO_4 and Fe, which is a result of the leaching of sulfate and whose presence is indicative of AMD. The practical result is that these ions create high conductivity values and, in consequence, low resistivity values (< 15 Ω m). For resistivity values between 15 and 130 Ω•m, rocks with an advanced state of alteration and high fracturing with the presence of water are expected. Resistivity values between 130 and 440 Ω m are correlable with massifs with a medium fracture stage and with light water percolation. For values above 440 Ω m, rocks with low fracturing and low degree of alteration - consequently low water movement are expected. Finally, values above 5000 Ω m represent unaltered and unsaturated masses.

Hydrogeochemical data from monitoring wells located along the pit provided by the company that manages the mining complex were also used. The analyses cover the main cations and anions present in the samples in addition to the physical-chemical parameters. These data confirm where AMD occurs (Fig. 5). Data from 11 monitoring wells were analyzed in addition to the waters of the pit lake. Groundwater samples were collected using the low-flow pumping methods described in the Brazilian standard—ABNT NBR 15847. The physical-chemical parameters (turbidity, dissolved oxygen, temperature, oxidation potential and pH) were analyzed using a Horiba U-23 multiparametric probe coupled to a flow cell.

The Mg, Ca, Si, Fe, Mn, Al, and Zn analyzes were determined by atomic emission spectrometry with an inductively coupled plasma source (ICP-OES), according to EPA-USEPA SW-846 6010/2007. The Cl^- ion was determined by the volumetric method, F^- was determined by the potentiometry method, K^+ and Na^+ were determined by atomic absorption—flame, NO_3 was determined using the methodology described by Mackereth et al. (1978), and SO_4 was determined by spectrometry with barium chloride. These data were kindly provided by the INB Company.

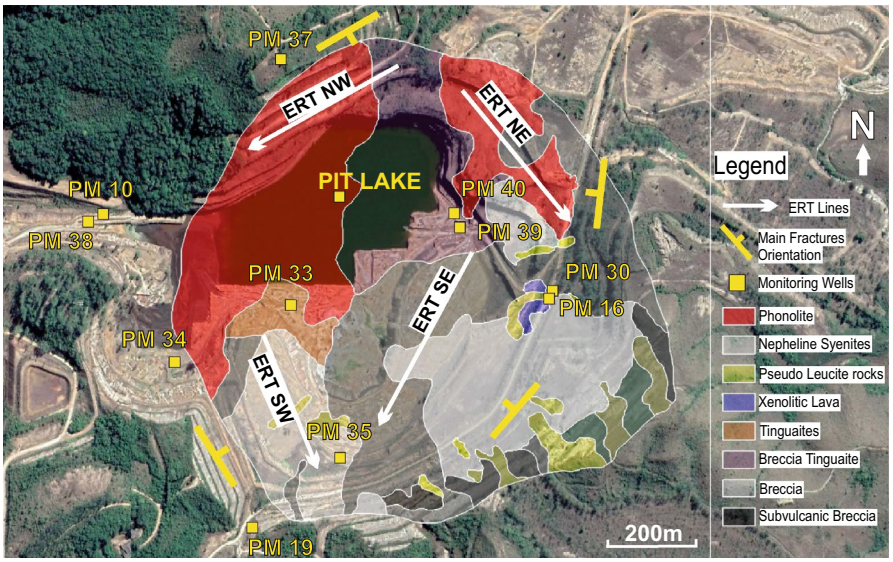

Fig. 6 Lithological map of the pit, positioning of the ERT lines, location of the monitoring wells and main orientation of discontinuities

Results and Discussion

The physical and chemical parameters of the monitoring wells are shown in Table 1, while the main cations and anions are presented in Tables 2, 3 and 4. Table 5 presents topographic data from the monitoring wells. The wells were ordered by each front and the different colors of the tables group the wells by fronts: SE, SW, NW, and NE.

The SE Front

The SE front was the largest, with a slope orientation of NE–SW with a high dip towards the center of the pit (NW). The main fracturing direction of the front is N25E/70NW (Fig. 6b). There are several points of the massif with the intense presence of vegetation and kaolinite, as well as points of the massif with continuous flow of water (Fig. 6a). ERT was tested in a more central portion

Table 1 Physical and chemical parameters; (*1 = 2013 data, *2 = 2014 data, *3 = 2015 data; PL = Pit Lake)

Well	DO (mg/L)			Turbidity (NTU)			Eh (V)			Cond. µS/cm			pH			Front
	*1	*2	*3	*1	*2	*3	*1	*2	*3	*1	*2	*3	*1	*2	*3	
16	6.97	6.29	6.07	1.3	9.9	10.3	0.20	0.26	0.38	53	60	114	5.4	6.0	4.7	SE
30	4.92	3.80	3.31	0.0	3.8	2.0	0.26	0.23	0.37	95	106	103	5.4	4.8	4.9	SE
35	2.41	1.44	0.78	0.0	3.7	1.5	0.41	0.31	0.39	157	236	233	4.5	4.2	3.8	SE
19	2.86	2.88	3.07	0.0	4.4	2.4	0.14	0.23	0.17	41	44	37	6.3	6.3	5.4	SW
33	0.23	0.18	0.28	9.7	6.9	23.6	0.22	0.19	0.37	6840	6670	6620	3.8	3.1	2.9	SW
34	2.74	3.77	3.70	0.0	4.0	2.0	0.13	0.25	0.15	373	406	362	5.5	5.3	4.5	SW
10	4.28	2.38	3.85	1.1	9.2	19.2	0.32	0.23	0.41	92	118	83	4.7	6.1	4.5	NW
37	6.78	5.29	7.98	0.0	0.0	1.5	0.22	0.00	0.20	13	13	14	5.6	5.2	5.4	NW
38	0.35	0.44	0.63	0.0	15.4	15.1	− 0.21	− 0.23	− 0.20	595	1034	593	7.4	8.6	9.0	NW
39	2.94	0.29	1.25	0.0	1.1	5.8	0.21	0.29	0.40	638	819	607	3.9	5.5	4.1	NE
40	0.56	0.98	1.10	24.7	25.3	14.0	− 0.03	− 0.02	− 0.02	909	968	933	6.7	5.1	5.4	NE
PL	7.90	6.70	7.28	12.0	8.7	14.0	0.37	0.37	0.37	1920	1800	1810	4.1	4.0	4.0	–

Table 2 Measured cations and anions—unit mg/L; (*1 = 2013 data, *2 = 2014 data, *3 = 2015 data; PL = Pit Lake)

Well	Ca			K			Na			Mg			F			Front
	*1	*2	*3	*1	*2	*3	*1	*2	*3	*1	*2	*3	*1	*2	*3	
16	2.9	3.4	2.4	4.3	3.6	4.9	0.2	0.1	0.2	0.2	0.3	0.2	2.1	0.5	2.1	SE
30	4.5	4.9	3.9	7.7	7.2	7.9	0.4	0.1	0.4	0.3	0.2	0.8	1.4	0.5	2.3	SE
35	10.1	9.4	10.4	9.2	8.4	9.6	0.2	0.1	0.3	0.4	0.3	0.4	7.9	2.9	12.9	SE
19	0.68	0.9	0.3	11.0	10.3	10.7	0.3	0.1	0.6	0.1	0.1	0.2	0.9	0.5	0.9	SW
33	337	344	258	81.8	80	66.0	3.0	3.7	1.7	30.2	28.0	31.2	0.9	0.5	0.9	SW
34	38.9	38.3	36.2	34.1	34.8	30.7	1.0	0.1	0.9	5.7	4.4	6.7	1.9	0.8	3.1	SW
10	7.5	8.9	5.1	3.9	3.7	3.6	0.4	0.3	0.4	0.5	0.5	0.5	1.7	0.6	0.8	NW
37	0.3	0.3	0.3	2.5	1.9	2.7	0.2	0.1	0.4	0.2	0.2	0.2	0.7	0.5	0.7	NW
38	82.2	96.4	67.2	10.6	11.8	8.0	5.5	1.8	8.4	0.5	1.0	0.1	4.4	4.9	4.0	NW
39	41.3	40.4	40.6	12.2	12.1	11.9	0.5	0.1	0.9	4.8	3.8	5.6	21.9	5.7	31.4	NE
40	152	138	158	61.4	58.6	60.7	2.4	2.8	1.8	7.3	6.8	7.5	4.2	3.5	4.9	NE
PL	510	584	437	13.1	13.6	12.7	0.7	0.1	1.4	16.1	10.8	16.7	8.1	2.1	14.2	–

Table 3 Measured cations and anions—unit mg/L; (*1 = 2013 data, *2 = 2014 data, *3 = 2015 data; PL = Pit Lake)

Well	CO_3			HCO_3			Cl			SO_4			NO_3			Front
	*1	*2	*3	*1	*2	*3	*1	*2	*3	*1	*2	*3	*1	*2	*3	
16	0	0	0	0	1	0.7	< 3	< 3	< 3	19	19	21	0.8	0.9	0.7	SE
30	0	0	0	0	0	0.0	< 3	< 3	< 3	32	33	38	2.2	2.1	2.3	SE
35	0	0	0	0	0	0.0	< 3	< 3	< 3	53	53	58	0.2	0.2	0.2	SE
19	0	0	0	9.2	12.1	0.4	< 3	< 3	< 3	0.7	0.5	0.0	6.4	6.2	5.8	SW
33	0	0	0	0	0	0.0	< 3	< 3	< 3	8523	7796	8424	0.5	0.1	0.8	SW
34	0	0	0	0	0	0.0	< 3	< 3	< 3	217	164	131	1.7	2.2	1.1	SW
10	0	0	0	0	0	0.0	< 3	< 3	< 3	45	34	48	1.6	2.6	0.4	NW
37	0	0	0	0.9	2.9	3.0	< 3	< 3	< 3	0.9	0.5	0.0	0.8	1.1	0.8	NW
38	0	0	0	41.8	61.4	12.8	< 3	< 3	< 3	248	223	220	0.4	0.2	0.5	NW
39	0	0	0	0	0	0.0	< 3	< 3	< 3	192	265	246	0.2	0.3	0.1	NE
40	0	0	0	10.9	0	1.8	< 3	< 3	< 3	499	401	476	0.1	0.1	0.1	NE
PL	0	0	0	0	0	0.0	< 3	< 3	< 3	1395	1254	1198	0.1	0.1	0.2	–

Table 4 Measured cations and anions—unit mg/L; (*1 = 2013 data, *2 = 2014 data, *3 = 2015 data; PL = Pit Lake)

Well	Si			Al			Fe			Mn			Zn			Front
	*1	*2	*3	*1	*2	*3	*1	*2	*3	*1	*2	*3	*1	*2	*3	
16	6.7	6.4	7.0	1.1	0.9	1.3	0.1	0.1	0.1	0.5	0.4	0.5	0.2	0.1	0.2	SE
30	9.1	8.5	9.4	2.7	2.8	2.6	0.1	0.1	0.1	1.1	0.9	1.2	0.2	0.2	0.2	SE
35	16.2	14.4	17.3	5.7	4.9	5.9	0.1	0.1	0.1	1.0	1.8	0.1	2.1	1.1	2.1	SE
19	9.1	8.0	9.4	0.0	0.1	0.0	0.0	0.0	0.0	0.0	0.0	0.1	0.1	0.1	0.1	SW
33	71.7	59.3	68.8	1019	1010	810	1148	1160	890	105	28.0	160.8	70.3	91	70.3	SW
34	17.8	16.0	18.3	3.8	2.3	5.0	0.6	0.6	0.5	8.4	4.4	11.7	3.6	3.4	3.6	SW
10	7.0	6.1	7.0	2.9	2.2	3.1	0.5	0.8	0.2	3.0	3.1	2.5	0.4	0.3	0.4	NW
37	5.4	4.1	5.8	0.3	0.1	0.3	0.4	0.4	0.0	0.1	0.2	0.0	0.0	0.0	0.0	NW
38	8.5	7.7	8.2	1.5	0.4	0.5	2.9	0.2	1.0	0.1	0.2	0.1	0.0	0.0	0.0	NW
39	14.4	12.5	15.6	16.7	31.7	29.6	13.8	20.1	22.5	11.1	17.3	19.6	2.7	2.8	2.7	NE
40	15.4	13.9	15.9	2.3	2.2	2.2	13.8	5.5	21.2	22.0	22.4	20.3	1.2	1.1	1.2	NE
PL	9.1	7.6	10.6	21.2	19.3	23.0	1.2	1.7	0.7	43.3	49.9	36.6	3.4	3.8	3.4	–

Table 5 Topographic data from monitoring wells

Monitoring well	Wellhead level (m)	Bottom level (m)	Water level (m)			Front
			2013	2014	2015	
16	1366	1360	1364.9	1364.7	1327.3	SE
30	1366	1342	1285	1285	1365	SE
35	1349	1343	1346.7	1346.6	1374.8	SE
19	1383	1359	1375.9	1373.9	1329.7	SW
33	1337	1319	1333	1327.8	1330.7	SW
34	1333	1321	1331.9	1330.5	1346.5	SW
10	1335	1323	1330.1	1327.3	1284.8	NW
37	1448	1412	1430.1	1428.9	1429.7	NW
38	1333	1303	1327	1324.4	1324.2	NW
39	1335	1323	1333.1	1332.7	1332.9	NE
40	1334	1286	1334	1331.7	1334	NE
Pit Lake	1331	–	1331	1331	1331	–

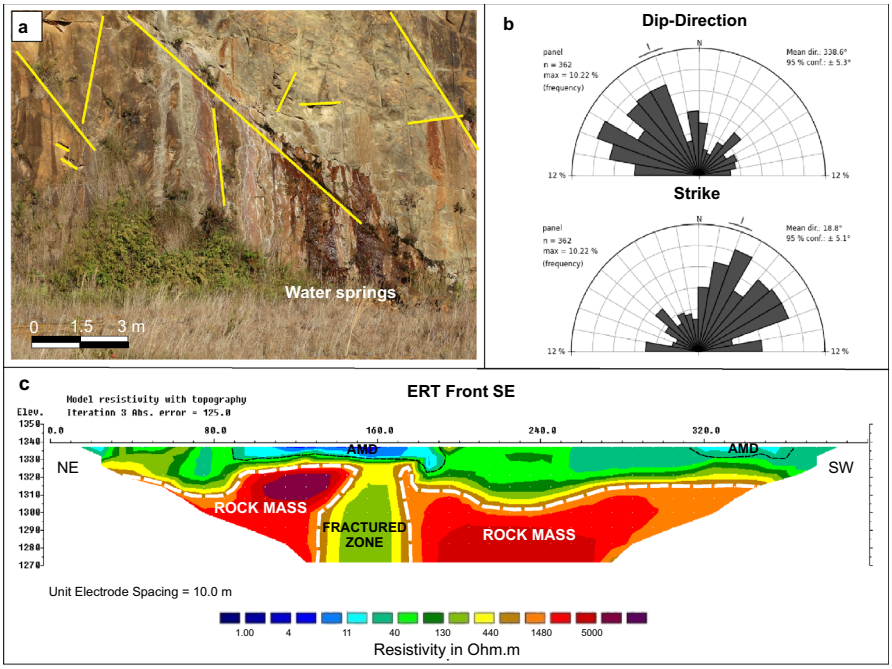

Fig. 7 **a** Presence of fractures in the massif and water springs at the base of the slope; **b** structural data; **c** ERT of front SE

of the mine pit, closer to the pit lake. The predominant lithology in this location is breccia pipe.

Between the topographic elevation of the ERT at 1340 m and the approximate elevation of 1315 m, it is possible to identify an upper portion of the figure associated with rocks with a greater degree of alteration and fracturing, and resistance values < 440 Ω m (Fig. 6c). Next to the 160 m electrode, there is a subverticalized structure that follows the same pattern of electrical resistivity. This structure possibly represents subvertical fractures associated with breccia pipe accommodation and movement, although it is not the main fracturing system. This entire region has water percolation, as shown by the continuous flow of water.

The variation of zones of high (> 1000 Ω m) and relatively low (< 100 Ω m) resistivity indicates the different stages of alteration and fracturing of the massif, but in general it is possible to say that below the 1310 m level (see Fig. 6c), there is a decrease in water percolation and, consequently, less permeability, with the exception of the indicated subvertical fractured zone. Another important factor is the presence of < 40 Ω m zones in the upper portion of the figure, which characterizes AMD.

There are three monitoring wells on the SE front. Two of them are far from the location of the ERT SE line. Wells 16 and 30 are located at a higher elevation (1366 m—top of the well head) than the ERT (1340 m). The presence of low pH in these respective wells, associated with the fracture

pattern of the massif with a dip in the center of the pit, indicates that this acidic drainage may surface at a lower level; the ERT may have intercepted one of these zones. Well 33, also acidic, is located closer to the ERT SE, and the chemical data can be correlated with the AMD zone at the end of the line at the SW ERT segment. The high values of conductivity (> 6600 µS/cm) and high concentration of sulfate (> 7700 mg/L) are also evidence of AMD.

The SW Front

The SW front slope has a NW–SE orientation and NE-plunge. There are two main fracturing systems: a fracture pattern with N20E/65SE attitude and another with N50W/85NE attitude (Fig. 7b), where there is also evidence of water percolation with the presence of kaolinite (Fig. 7a). The SW ERT was only 300 m long due to the limited space between pit benches (Fig. 7c). The local lithology is a variation of pipe breccia with syenites.

There is a large area of high resistivity in the 1320 m elevation that extends from the beginning of the SW ERT to 190 m, which was interpreted as unsaturated and unchanged rock mass. However, the body's morphology indicates a vertical contact and the presence of subvertical fractures, suggesting the typical rocks had contacted the fractured pipe—breccia pipe (≈ 400 Ω m). In the fracture that marks the lithological contact, there is water percolation with low resistivity values, indicating AMD. Acid drainage is present in the upper portion of the figure above the 1320 m elevation, which suggests intense water movement closer to the surface.

This water movement closer to the surface also favors oxygenation, an important factor in the genesis of AMD. This was confirmed by the proximity to well 33, which has acidic characteristics. Wells 34 and 19 are located at a greater distance from ERT SW than well 33, so for purposes of correlation, well 33 is more appropriate. Another important observation is that well 33 is located ≈ 100 m from the pit lake, which acts as a large collector of meteoric and underground waters. The concentration values of the Ca ion is > 258 mg/L, which is a relatively high value compared to al lof the other monitoring wells, though less than the value of the pit lake, which ranges from 437 to 584 mg/L. The high concentration of this ion is due to the disposal of DUCA in the pit area; the high values in well 33 suggest communication between this well and the lake, resulting from the massif's high permeability.

The NW Front

The NW front slope has a NE–SW orientation and strikes to the SE. There are two main fracture systems: a fracture pattern with N35E/75NW attitude and another with N85E/75SE attitude (Fig. 8b). The NW front has shorter benches and more vertical slopes. There is constant water flow in the massif and the presence of kaolinite veins and more developed vegetation (Fig. 8a). Local lithology is composed of phonoliths and breccia.

In the central and lower portion of Fig. 8c, there is a large zone of high resistivity with values > 1400 Ω m, which represents a less fractured and almost unaltered massif. From the 260 m electrode, there is a well-defined property contrast.

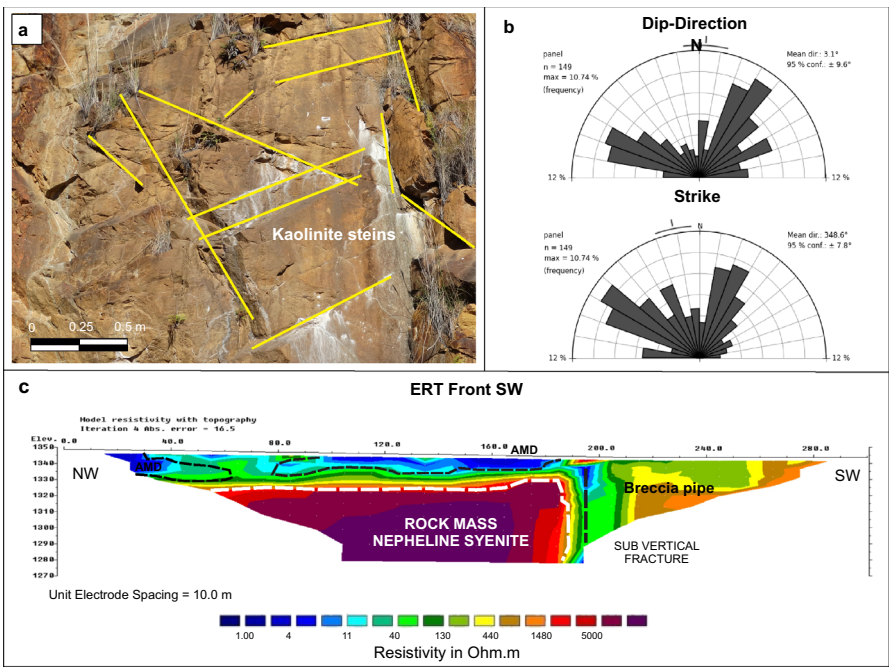

Fig. 8 **a** Presence of fractures in the massif and kaolinite steins; **b** structural data; **c** ERT of the SW front

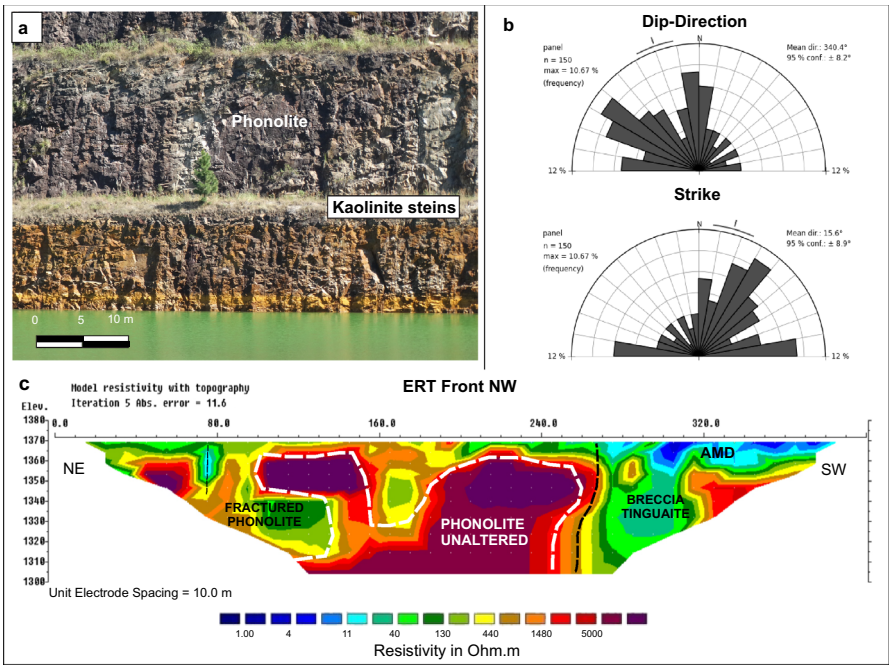

Fig. 9 **a** Presence of fractures in the massif and kaolinite steins; **b** structural data; **c** ERT of the NW front

This contrast reflects a local lithological contact between the less fractured phonoliths with the brecciated rocks, which have a higher degree of alteration and fracturing. The breccia probably hosts mineralization and pyritization, as evidenced by the presence of AMD in the final portion of the line, starting from the 260 m electrode.

The most representative monitoring well on the NW front is well 37. Its slightly acidic character reflects the minimal influence of AMD in the upper portion of the massif. However, as the water percolates along the slope, the tendency is for it to acidify, especially in the more mineralized portions. Monitoring wells 10 and 38 are located side by side close to the drainage area of the pit lake and have different pHs. While well 10 is acidic (pH values between 4.5 and 6.1), well 38 is alkaline (pH values between 7.4 and 9.0). This distinction can be explained by the difference in the bottom level of each well. Well 10 has a total length of only 12 m (top level = 1335 m; bottom level = 1323 m); because it is shallower, it is under the influence of the most superficial area of the massif where the rocks are more permeable. It is acidic due to its proximity to the lake's acidic water. Well 38, on the other hand, is deeper (top level = 1333 m; bottom level = 1303 m) and has less percolation of meteoric water because the rock is less fractured at greater depths and, consequently, has less permeability.

Targa et al. (2021) demonstrated that there is a small influence of surface water in well 38, including contaminated water from the DUCA treatment waste located nearby. Although the contaminated water flow is low, it is enough to change the physicochemistry, which would explain its relatively high turbidity.

The NE Front

The NE front slope has a NW–SE orientation and SW strike direction. The main fracture pattern has an attitude of N5E/85NW (Fig. 9b). The NE front has more scattered benches and less vertical slopes. The local lithology is composed of fractured phonolites and syenites. It was the only front in which there was no evidence of water flow through the massif (Fig.9a). Before exploitation of the pit began, the NE region had a high topography and was the head of the local hydrographic basins. The pit is located between the Consulta stream basin to the east and the Cercado stream basin to the west. Even today, the NE front disperses part of the water to the east, while the other fronts disperse water to the west.

Figure 9c shows two zones of greater electrical resistance (> 1000 Ω m) associated with the syenites. With the exception of areas with high resistivity, there are no other areas with high contrasts. According to the geological mapping of the mine pit, this area with intermediate resistivity is likely a highly fractured phonolite sill. In the central portion, it is still possible to identify a fractured phonolite dike. There is no evidence of AMD at the ERT NE survey site.

In the NE front, there are two monitoring wells: 39 and 40—both with low pH. Although the geophysical lines do not show evidence of AMD, these wells are likely contaminated due to the influence of drains from other fronts, such as the SE front. The two NE wells are located side by side next to the pit lake. Well 39 is shallower than 40 and, like the NW front, the difference in these pH values (Well 39 pH values between 3.9 and 5.5; Well 40 pH values between 5.1 and

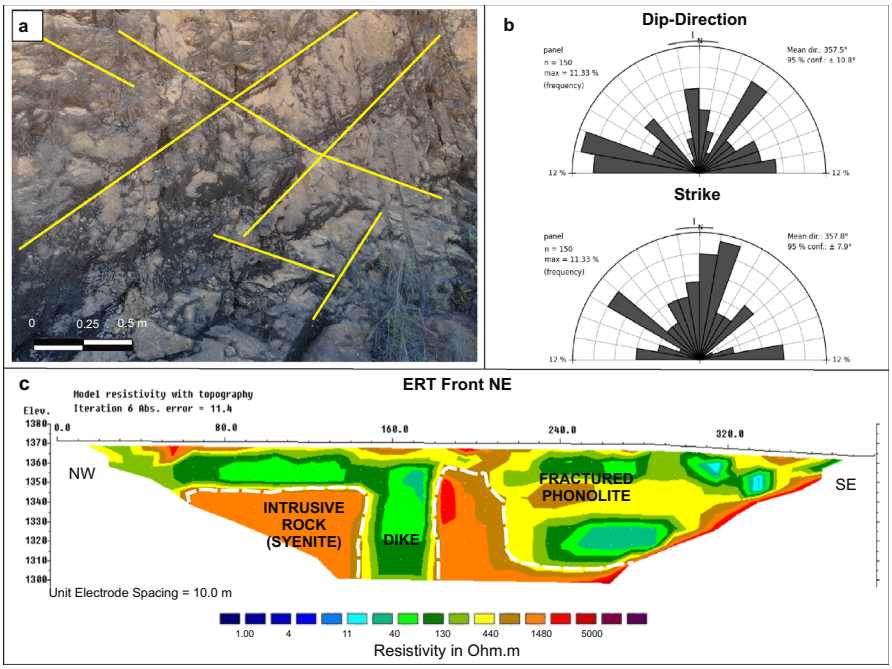

Fig. 10 **a** Presence of fractures in the massif; **b** structural data; **c** ERT front NE

6.7) can be explained by the percolation and permeability of the shallow rocks in the deeper portions of the massif. It is important to note that the NE front portion was intensively mined and so there may be a greater level of ore depletion.

Conclusions

The combination of intense fractures and mineralized zones at the Osamu Utsumi mine provides ideal conditions for the generation of acid drainage. In 1995, the company responsible for the commercial exploitation of the uranium decided to close the mine because extraction was no longer economically viable.

The pit is the largest environmental liability of the mining complex because it is a deep depression that conducts both meteoric water and groundwater that seeps through the massif's local fracture pattern and is contaminated by mineralized zones. A geometric structural analysis of the pit revealed a complex framework in which all of the operating fronts have the main fracture pattern with a strike into the center of the pit.

Fractures with water flow or signs of percolation were verified on the SE, SW and NW fronts, as described by Targa et al. 2019. This demonstrates the clear influence of the discontinuities on the flow of underground water and corroborated the source of the acid drainage, since the mineralized and sulfide-rich areas are directly related to the intense fracturing of the area and the mineral genesis of the deposit.

The ERT surveys efficiently identified fractured zones with acid water percolation by their very low electrical resistivity (< 15 Ω m). Many of the conclusions indicated by the geophysical method were validated by the geochemical data. An integrated analysis of the chemical data, taking into consideration that some wells located side by side had different depths, allowed a very comprehensive understanding of the environmental aspects of the mine pit. It was also possible to identify well-marked lithological contacts.

The geophysical and structural geology data made it possible to identify areas where fracture patterns intersected. These fractured zones are very permeable and conduct groundwater more effectively, like a natural gutter. In the field, it was possible to conclude that several fractures had water flowing through them, but the geophysical data indicated that not all of these fractures contained AMD.

The long-term environmental liability of the Osamu Utsumi mine is a complex problem, since today the treatment of effluents is carried out in a palliative way and seeks only to alleviate the effects of the problems. The ideal alternative would be to directly address the cause of the problem and for that, the first step was to identify the main areas of AMD generation. The mapping of acid-generating areas makes it is possible to propose geotechnical solutions to the problem, such as preventing water from seeping through mineralized (sulphidized) areas. Since the water in the massif percolates through the fractures present in it, one potential option would be a ground treatment, e.g. jet-grouting, directly into areas of greater permeability. The results of this work indicate that the zones of influence of AMD are limited to a depth of up to 35 m from the land surface, which makes

the aforementioned option technically feasible. Other alternatives to decrease the permeability would be perforations with injections of bentonite and / or synthetic polymers.

This study allowed us to map the areas that generate acid drainage. This is the first stage for long-term preventive measures. However, for greater treatment efficiency, we recommended that more geophysical surveys be carried out to provide more detail of the entire pit, due to its size.

Acknowledgements This study was financed in part by the Coordenação de Aperfeiçoamento de Pessoal de Nível Superior - Brasil (CAPES) - Finance Code 001. The authors thank Coordenação de Aperfeiçoamento de Pessoal de Nível Superior (CAPES), the Foundation for Research Support of the State of Sao Paulo (Fundação de Amparo a Pesquisa do Estado de São Paulo - FAPESP) and the INB for their support.

References

ABEM (2012) Terrameter LS—instruction manual. Sundbyberb, Sweden

ABNT NBR (Brazilian Association of Technical Standards) 15847 (2010) Amostragem de água subterrânea em poços de monitoramento—Métodos de purga. ABNT, Rio de Janeiro (**In Portuguese**)

Biondi JC (2015) Processos metalogenéticos e os depósitos minerais brasileiros. Oficina de texto, São Paulo (**In Portuguese**)

Buselli G, Lu K (2001) Groundwater contamination monitoring with multichannel electrical and electromagnetic methods. J Appl Geophys 48:11–23

Cipriani M (2002) Mitigação dos impactos sociais e ambientais decorrentes do fechamento definitivo de minas de urânio. PhD Diss, Univ of Campinas **(In Portuguese)**

Côrtes ARP, Moreira CA, Veloso DIK, Vieira LB, Bergonzoni FA (2016) Geoelectrical prospecting for a copper-sulfide mineralization in the Camaquã sedimentary basin, southern Brazil. Geofis Int 55(3):107–117

Degroot-Hedlin C, Constable S (1990) Occam`s inversion to generate smooth, two-dimensional models form magnetotelurric data. Geophysics 55(12):1613–1624

Ebraheem AM, Hamburger MW, Bayless ER, Krothe NC (1990) A study of acid mine drainage using earth resistivity measurements. Groundwater 28(3):361–368

Edwards LSA (1977) A modified pseudosection for resistivity and induced polarization. Geophysics 42(5):1020–1036

Epov MI, Yurkevich NV, Bortnikova SB, Karin YG, Saeva OP (2017) Analysis of mine waste by geocheimical and geophysical methods (a case study of the mine tailing dump of the Salair ore-processing plant). Russ Geol Geophys 58:1543–1552

Fernandes HM, Veiga LHS, Franklin MR, Prado VCS, Taddei JF (1995) Environmental impact assessment of uranium mining and milling facilities: a study case at the Poços de Caldas uranium mining and milling site. Brazil. J Geochem Explor 52:161–173

Fraenkel MO, Santos RC, Loureiro FEVP, Muniz WS (1985) Jazida de urânio no planalto de Poços de Caldas. Minas Gerais. DNPM. Principais depósitos minerais do Brasil. Recursos Minerais Energéticos 1(5):89–103

Franklin MR (2007) Modelagem numérica do escoamento hidrológico e dos processos geoquímicos aplicados à previsão da drenagem ácida em uma pilha de estéril da mina de urânio de Poços de Caldas, MG. PhD Diss, Univ Federal of Rio de Janeiro **(In Portuguese)**

Frid V, Averbach A, Frid M, Dudkinski D, Liskevich G (2017) Statistical analysis of resistivity anomalies caused by underground caves. Pure Appl Geophys 174:997–1012. https://doi.org/10.1007/s00024-015-1106-x

Garda MG (1990) A alteração hidrotermal no contexto da evolução geológica do maciço alcalino de Poços de Caldas, MG-SP. MSc thesis, Univ of São Paulo **(In Portuguese)**

Gélis C, Revil A, Cushing EM, Jougnot D, Lemeille F, Cabrera J, De Hoyos A, Rocher M (2010) Potential of electrical resistivity tomography to detect fault zones in limestone and argillaceous formations in the experimental platform of Tournemire. France Pure Appl Geophys 167:1405–1418

Gélis C, Noble M, Cabrera J, Penz S, Chauris H, Cushing EM (2015) Ability of high-resolution resistivity tomography to detect fault and fracture zones: application to the Tournemire experimental platform of France. Pure Appl Geophys 173:573–589

Ghosal S, Singh A, Agrahari S, Sengupta D (2020) Delineation of heavy mineral bearing placers by electrical resistivity and radiometric techniques along coastal Odisha. India. Pure Appl Geophys 177:4913–4923. https://doi.org/10.1007/s00024-020-02502-3

Gómez-Ortiz D, Martín-Velazquez S, Matín-Crespo T, De Ignácio-San José C, Lillo J (2010) Application of electrical resistivity tomography to the environmental characterization of abandoned massive sulphide mine ponds (Iberian Pyrite Belt. SW Spain). Near Surf Geophys 8:65–74

Hamdan H, Andronikidis N, Kritikakis G, Economou N, Agioutantis Z, Schilizzi P, Steiakakis C, Papageorgiou C, Tsourlos P, Vargemezis G, Vafidis A (2014) Contribution of electrical tomography methods in geotechnical investigations at Mavropigi lignite open pit mine, northern Greece. Environ Earth Sci 72(5):1589–1598

Holmes DC, Pitty AE, Noy DJ (1992) Geomorphological and hydrogeological features of the Poços de Caldas caldera analogue study sites. J Geochem Explor 45:215–247

Kearey P, Brooks M, Hill I (2002) An introduction to geophysical exploration. Wiley, Hoboken

Khalil MA, Bobst A, Mosolf J (2018) Utilizing 2D electrical resistivity tomography and very low frequency electromagnetics to investigate the hydrogeology of natural cold springs near Virginia City. southwest Montana. Pure Appl Geophys 175:3525–3538. https://doi.org/10.1007/s00024-018-1865-2

Korneeva T. Yurkevich N. Jucher D. Saeva O (2016) Geochemical and geophysical characterization of acid mine drainage and sulfide tailings at karabash mine site (South Ural. Russia). Int J Adv Res Sci Eng Technol 4(1):114–120

Legault JM, Carriere D, Petrie L (2008) Synthetic model testing and distributed acquisition dc resistivity results over an unconformity uranium target from the Athabasca Basin, northern Saskatchewan. Geophysics 27:46–51

Lghoul M, Teixidó T, Peña JA, Hakkou R, Kchikach A, Guérin R, Jaffal M, Zouhri L (2012) Electrical and seismic tomography used to image the structure of a tailings pond at the abandoned Kettara Mine. Morocco. Mine Water Environ 31:53–61. https://doi.org/10.1007/s10230-012-0172-x

Loke MH, Baker RD (1996) Rapid least-squares inversion of apparent resistivity pseudosections by quasi-Newton method. Geophys Prospect 44(1):131–152

Mackereth FJH (1978) Water analysis: some revised methods for limnologists. Titus Wilson & Son, Ltd, Kendal

Magno LB Jr (1985) Osamu Utsumi Mine. Geologic Presentation. In: Intern report of NUCLEBRÁS **(In Portuguese)**

Mandal A, Biswas A, Mittal S, Mohanty WK, Sharma SP, Sengupta P, Sen J, Bhatt AK (2013) Geophysical anomalies associated with uranium mineralization from Beldih Mine. South Purulia shear zone. India. J Geol Soc India 82:601–606

Martín-Crespo T, Gómez-Ortiz D, Martín-Velázquez S, Martínez-Pagán P, De Ignacio C, Lillo J, Faz A (2018) Geoenvironmental

characterization of unstable abandoned mine tailings combining geophysical and geochemical methods (Cartagena-La Union district. Spain). Eng Geol 232:135–146. https://doi.org/10.1016/j.enggeo.2017.11.018

Martínez-Pagán P, Faz A, Aracil E, Arocena JM (2009) Electrical resistivity imaging revealed the spatial properties of mine tailing ponds in the Sierra Minera of southeast Spain. J Environ Eng Geophys 14:63–76

Martínez-Pagán P, Gómez-Ortiz D, Martín-Crespo T, Manteca JI, Rosique M (2013) The electrical resistivity tomography method in the detection of shallow mining cavities. A case study on the Victoria Cave. Cartagena (SE Spain). Eng Geol 156:1–10. https://doi.org/10.1016/j.enggeo.2013.01.013

Martínez-Pagán P, Gómez-Ortiz D, Martín-Crespo T, Matín-Velázquez S, Matínez-Segura M (2021) Electrical resistivity imaging applied to tailings ponds: an overview. Mine Water Environ 40:285–297. https://doi.org/10.1007/s10230-020-00741-3

McNeill JD (1980) Electromagnetic terrain conductivity measurement at low induction numbers. Technical note TN-6. Geonics Ltd, Mississauga

Merkel RH (1972) The use of resistivity techniques to delineate acid mine drainage in ground water. Ground Water 10(5):38–42

Moon CJ, Whateley MEG, Evans AM (2006) Introduction to mineral exploration. Wiley, Hoboken

Moreira EC, Fernandes LED, Pereira VP (2007) A Análise de Lineamentos Estruturaiz. Sob a Óptica da Geometria Fractal, no Maciço Alcalino de Poços de Caldas (MG). Revista Pesquisa em Geociências 34(2):89–97 (**In Portuguese**)

Moreira CA, Lapola MM, Carrara A (2016) Comparative analyzes among electrical resistivity tomography arrays in the characterization of flow structure in free aquifer. Geofis Int 55(2):119–129

Moreira CA, Helene LPI, Nogara P, Ilha LM (2018) Analysis of leaks from geomembrane in a sanitary landfill through models of electrical resistivity tomography in South Brazil. Environ Earth Sci. https://doi.org/10.1007/s12665-017-7180-x

Moreira CA, Casagrande MFS, Siqueira Büchi FM, Targa DA (2020) Hydrogelogical characterization of a waste rock pile and bedrock affected by acid mine drainage from geophysical survey. SN Appl Sci 2:1236. https://doi.org/10.1007/s42452-020-3021-8

Mwenifumbo CJ, Elliot BE, Jefferson CW, Bernius GR, Pflug KA (2004) Physical rock properties from the Athabasca Group: designing geophysical exploration models for unconformity uranium deposits. J Appl Geophys 55:117–135

Obiadi II, Onwuemesi AG, Anike OL, Ajaegwu NE, Anakwuba EK, Nwosu CM, Akpunonu EO, Onuigbo EN, Onuba OL (2013) Determining subsurface fracture characteristics from the azimuthal square array resistivity survey at igarra. Niger Pure Appl Geophys 170:907–916. https://doi.org/10.1007/s00024-011-0443-7

Oliveti I, Cardarelli E (2019) Self-potential data inversion for environmental and hydrogeological investigations. Pure Appl Geophys 176:3607–3628. https://doi.org/10.1007/s00024-019-02155-x

Pires FRM (2013) Urânio no Brasil: geologia, jazidas e ocorrências. Eletrobrás Eletronuclear. Rio de Janeiro **(In Portuguese)**

Placencia-Gómez E, Parviainen A, Hokkanen T, Loukola-Ruskeeniemi K (2010) Integrated geophysical and geochemical study on AMD generation at the Haveri Au–Cu mine tailings. SW Finl Environ Earth Sci 61:1435–1447

Poisson J, Chouteau M, Aubertin M, Campos D (2009) Geophysical experiments to image the shallow internal structure and the moisture distribution of a mine waste rock pile. J Appl Geophys 67:179–192

Rucker DF, Glaser DR, Osborne T, Maehl WC (2009) Electrical resistivity characterization of a reclaimed gold mine to delineate acid rock drainage pathways. Mine Water Environ 28:146–157

Targa DA, Moreira CA, Camarero PL, Casagrande MFS, Alberti HLC (2019) Structural analysis and geophysical survey for hydrogeological diagnosis in uranium mine. Poços de Caldas (Brazil). SN Appl Sci 1:299. https://doi.org/10.1007/s42452-019-0309-7

Targa DA, Moreira CA, Casagrande MFS (2021) Hydrogeological analysis of sulfide tailings at a uranium mine using geophysical and hydrochemical methods. Mine Water Environ. https://doi.org/10.1007/s10230-021-00791-1

Tuncer V, Unsworth MJ, Siripunvaraporn W, Craven JA (2006) Exploration for unconformity-type uranium deposits with audiomagnetotelluric data: a case study from the McArthur River mine. Sask Can Geophys 71(6):201–209

Waber N, Schorscher HD, Peters T (1992) Hydrothermal and supergene uranium mineralization at the Osamu Utsumi mine, Poços de Caldas, Minas Gerais, Brazil. J Geochem Explor 45:53–112

Yuval D, Oldenburg W (1996) DC Resistivity and IP methods in acid mine drainage problems: results from the Copper Cliff mine tailings impoundments. Appl Geophys 34:187–198

Zhang G, Lü QT, Zhang GB, Lin PR, Jia ZY, Kui S (2018) Joint interpretation of geological, magnetic, AMT, and ERT data for mineral exploration in the northeast of inner Mongolia. China Pure Appl Geophys 175:989–1002. https://doi.org/10.1007/s00024-017-1733-5